Cogging Torque Analysis on PM-Machines by Simulation and Measurement

D. van Riesen, C. Schlensok, B. Schmülling, M. Schöning, K. Hameyer

Abstract — **Cogging torque is an effect to be considered in the design and optimization process of Permanent Magnet Machines (PMM). Many simulation methods have been proposed. Verification of provided results require measurements of the cogging torque. Measuring it is, though, no easy task. Existing measurement setups often do not decouple the influence of the drive and the measured PMM. Hence, we propose a simple yet accurate test bench design for the measurement of cogging torque. The studied PMM is simulated using the Finite Element Method (FEM), and the results are compared.**

Index Terms — **cogging torque, measurement, FEM, permanent-magnets machines.**

I. Introduction

MANY studies have been presented concerning the minimization of cogging torque in Permanent Magnet Machines (PMM) [1-4]. This states the high relevance of the cogging problematic in top quality PM-servo drives with high precision positioning ability and for standard mass produced PMMs as well. Therefore, the determination and estimation of the peak-to-peak cogging torque and the cogging harmonics are of high interest. Both, simulation and measurement allow for the analysis of the cogging torque. Simulation methods, i.e. the Finite Element Method (FEM), are well known and easy to apply [5,6]. Hence, the focus lies on the development of a precise but simple measurement setup allowing for accurate cogging torque analysis.

Various test-bench setups have been presented or are sold commercially. Nevertheless, there is at least one disadvantage to these. The setup presented in [8] consists of the PMM, a torque transducer and a hydraulic motor as drive. This configuration promises a very high accuracy of the rotor movement. There is no cogging or torque ripple in the hydraulic drive. Nevertheless, the setup works without any offset, so that the measurement is performed in a close range around the zero value. Next to this small disadvantage there is the cost aspect. The hydraulic drive is rather expensive and not easy to handle. Another setup, similar to the one presented in this paper, allows for accurate performance but also includes the problem of measuring around "0" [9]. A third alignment is very simple and rather inaccurate. The cogging is measured by weights being adjusted for each of the cogging positions [10]. There are a lot of unknown errors in this measurement setup.

II. Measurement Setup

The measurement setup is shown in Fig. 1. The PMM is mounted onto a flange and is connected with two flexible couplings to the torque transducer, a gear, and a stepper motor. Between the first coupling and the PMM there is a disc which holds a spindle with a weight.

The weight is used as offset torque. This way the measurement is performed in the range of about 1 Nm. The weight weighs 2 kg and the disc has a radius of 5 cm. The offset allows for the torque transducer to measure in its optimum scale range. The transducer's maximum torque is 2 Nm. The signal from the transducer is fed into a measurement control unit (MGC) which allows for digital signal processing, e.g. dSPACE [11]. The stepper motor driving the whole setup is controlled by two voltage sources. The resolution of the stepper motor can be switched from 1/1, 1/2, 1/4 to 1/8. By additionally varying the voltage from 0 – 8 V the speed can be adjusted from 0 to 64 rpm with a transmission ratio of the gear of 1/400. This high ratio avoids a measurable impact of the stepper motor's torque ripple to the cogging torque of the PMM. The harmonics of the stepper motor are very high and are filtered from the signal digitally by the software. Fig. 2 summarizes the setup schematically.

Due to the offset weight the average value of the measurement differ with the direction of rotation. Fig. 3 shows exemplarily the results for one PMM. It can be seen, that the friction is measured as well. The deviation of the average values of both measurements equals twice the friction of the entire setup. While the weight is spun upwards the friction works against the torque of the stepper motor. When the weight is moving downwards the friction works in the same direction. Fig. 4 shows the cleared cogging torque signal without friction and offset. The difference of the resulting time-dependent cogging-torque stems from the rotational direction of the stepper motor.

Manuscript received July 15th, 2006.

D. van Riesen, C. Schlensok, B. Schmülling, M. Schöning and K. Hameyer are with the Institute of Electrical Machines, RWTH Aachen University, D-52056 Aachen, Germany. (phone: +49-241-8097667; fax: +49-241-8092270; e-mail: dirk.vanriesen@ iem.rwth-aachen.de).

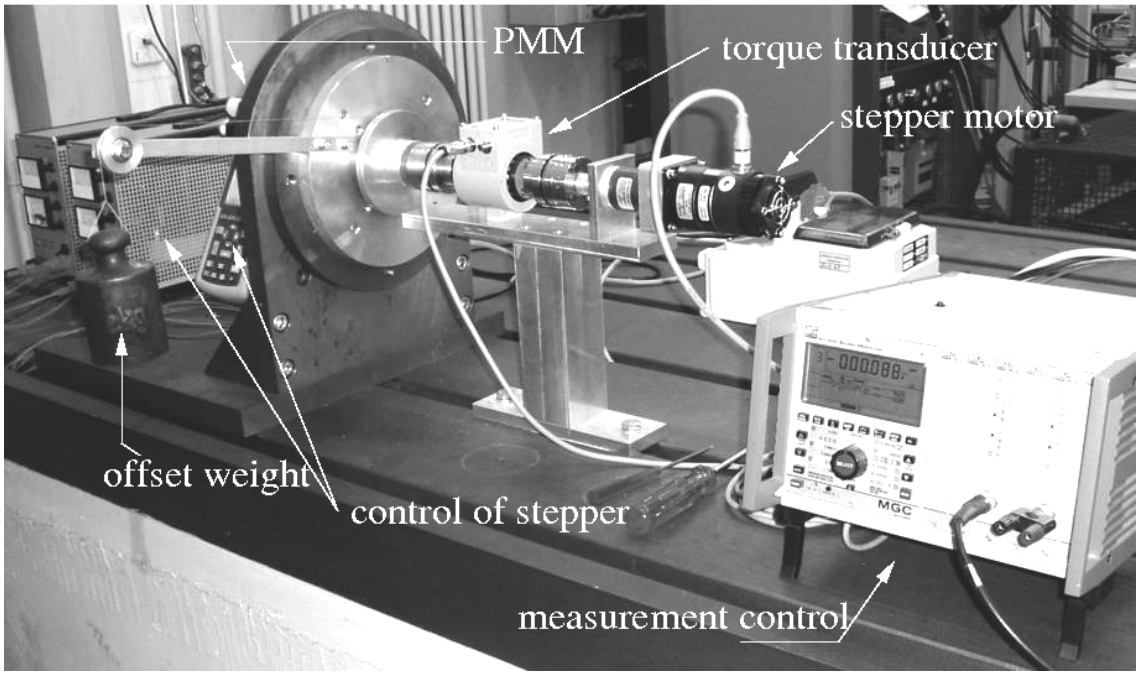

Fig. 1. Picture of the measurement setup in the lab.

III. Measurement Results

The measurement setup is tested with two different servo drives. Both are permanent-magnets synchronous machines. The setup allows for three complete rotor revolutions. This depends on the height of the test bench, since the cord of the weight is lowered until the weight touches the floor. For both PMMs the cogging torque is measured at 1 rpm in both directions of the weight. As studies have shown the selected speed of the stepper motor leads to accurate results, and an acceptable duration of 3 min of each of the measurements with an easy handling. Therefore, four different measurements are performed.

Two different cogging-torque analysis-criteria are usually applied:

1. the harmonic analysis of the cogging-torque, and
2. the peak-to-peak value of the cogging torque.

Both analysis criteria afford one complete rotor revolution.

At first the spectra of the four cogging torque behaviours are analysed in Fig. 5 and 6. For both machines the harmonics are nearly independent of the rotational direction of the stepper

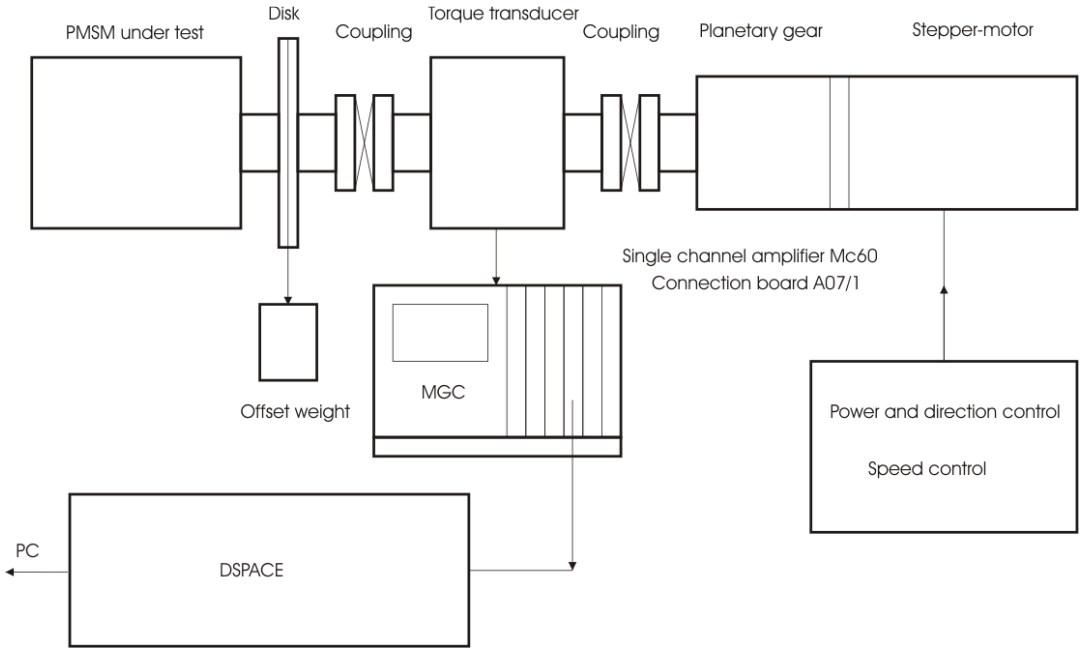

Fig. 2. Scheme of the measurement setup.

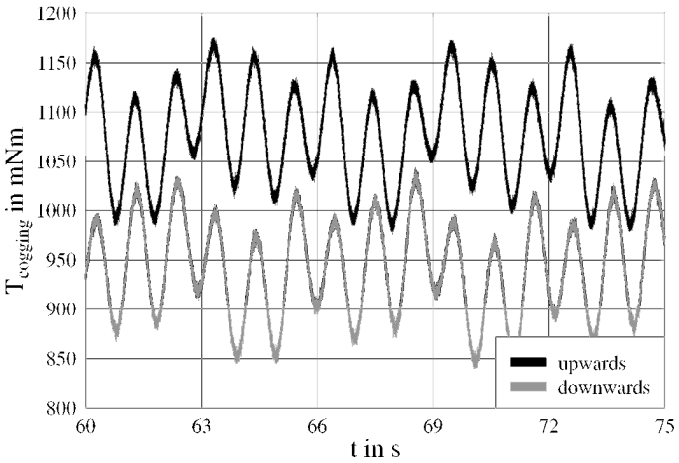

Fig. 3. Cogging torque results for both directions of stepper motor.

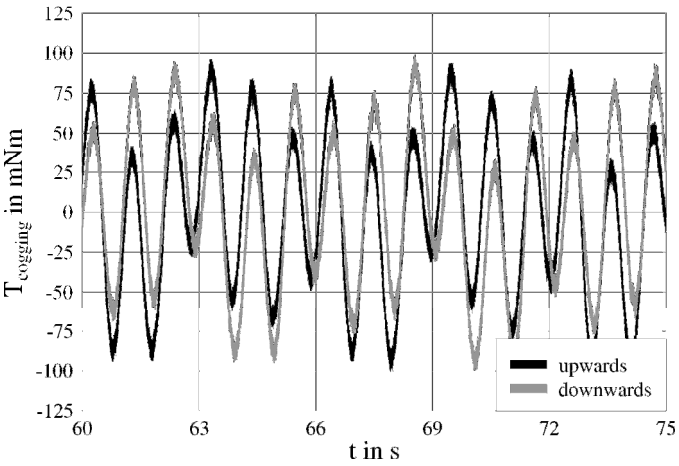

Fig. 4. Cogging torque results without offset and friction.

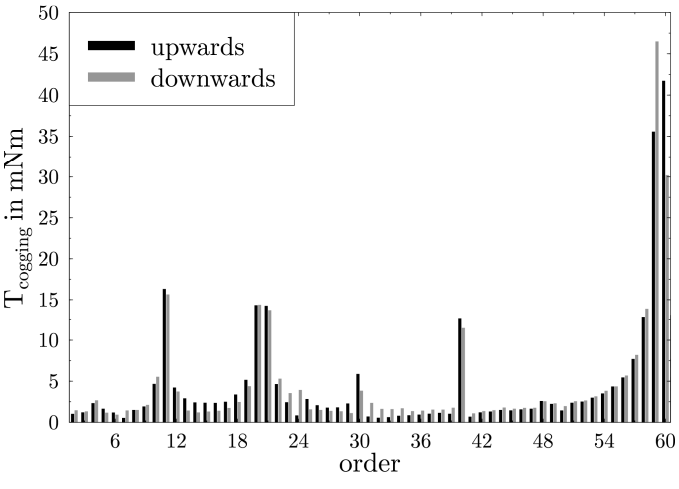

Fig. 5. Spectrum of the cogging torque for studied PMM **A**.

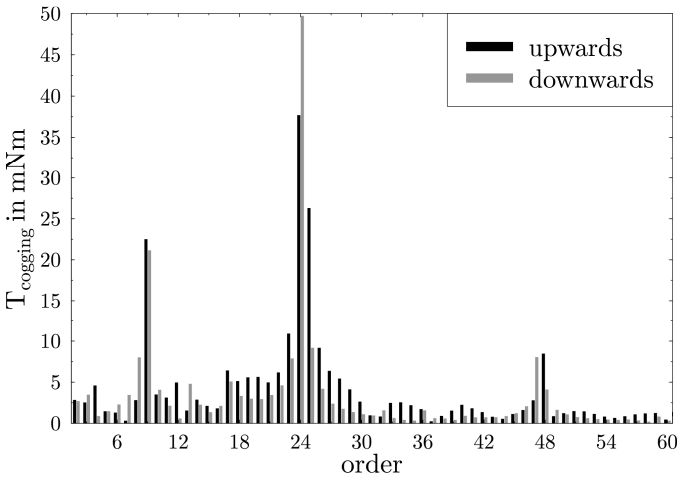

Fig. 6. Spectrum of the cogging torque for studied PMM **B**.

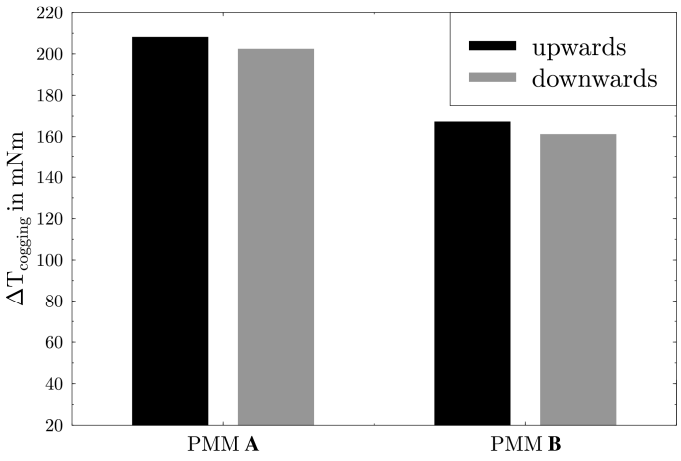

Fig. 7. Peak-to-peak cogging-torque values.

motor and match very well. Due to the different designs of both PMMs the occurring harmonics differ. For PMM **A** the dominant harmonic is order number 60. PMM **B** shows major mode number 24.

The peak-to-peak values of the cogging torque are shown in Fig. 7. It can be stated, that for each of the PMM the results are mostly independent of the rotational direction. PMM B has a lower cogging torque (-19.95 %).

The measurement setup has beend used to compare the cogging torque behaviour of the two PMMs, regarding them as "black boxes", since no construction data was available. Hence, no simulation could be performed, since the stator lamination design is unknown, as well as the rotor lamination and size and placement of the permanent magnets. Nevertheless, the measurement already allows to state a difference between the two machines, which could be used as a benchmark for applications where low cogging torque is a requirement.

Next, a different PMM (PMM **C**) was measured. For this machine, detailed drawings were available. Therefore, the measurements will be compared to simulated results. The machine is measured with the same measurement setup.

Again, a speed of 1 rpm is chosen, and the upward and downward movement of the counterweight is measured (resulting in clockwise and counter-clockwise rotation of the machine). Fig. 8 shows the measured torque values. It must be noted, that the curves are phase-shifted against each other, since the exact starting angle of the machine is not recorded and varies between measurements. But this has no effect on the determination of the peak-to-peak value or the spectrum analysis of the cogging torque.

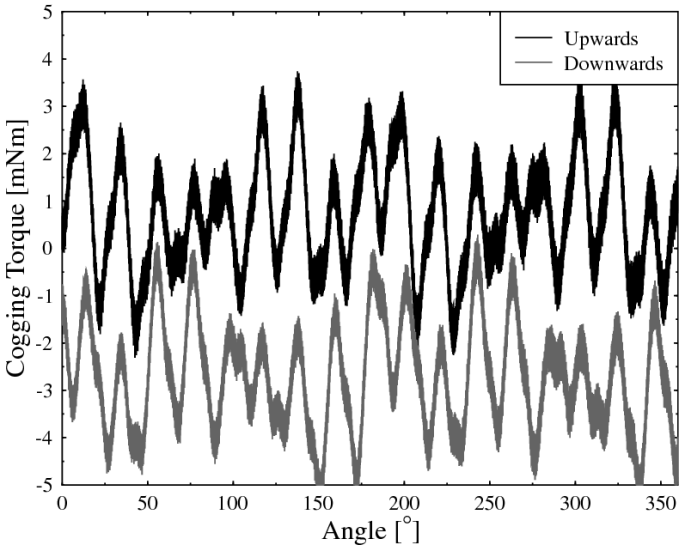

Fig. 8. Cogging torque measured in both directions for the PMM C

After determining the friction of the machine, it can be eliminated from the measured values, resulting in the time-dependent cogging torque shown in Fig. 9, which will serve as the starting point for the FFT analysis.

The FFT is performed, resulting in the spectrum depicted in Fig. 10. The most relevant order appearing in the spectrum is the 18th, which is in good agreement with the results expected from an analytical analysis. 18 is the least common multiple of the number of slots (18) and the number of rotor poles (6) (see next section). The 36th order is also clearly visible. Lower orders appear as well, due to asymmetries in the construction.

IV. Simulation Results

The electromagnetic simulation is applied to verify both the measurement setup and the FE-model. The solver tool used is iMOOSE [7] which has been developed at the Institute of Electrical Machines at RWTH Aachen University in the past few years. The PMM **C** is used for the simulation. It consists of N_S = 18 stator teeth and $2p$ = 6 rotor poles. The lamination

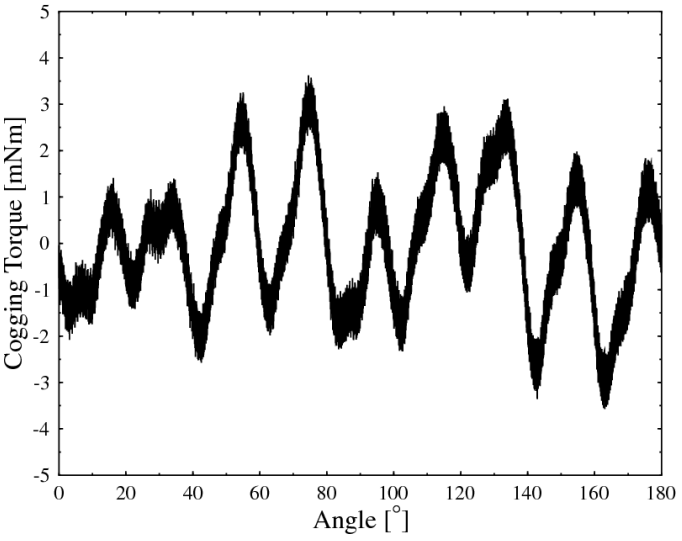

Fig. 9. Cogging torque for PMM C with friction eliminated.

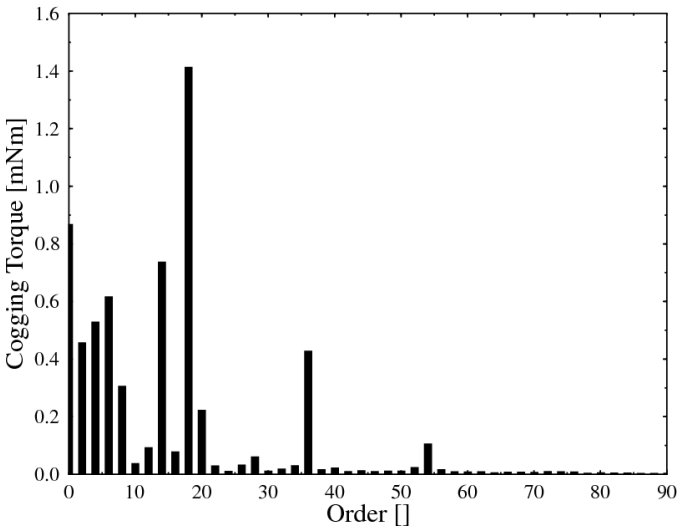

Fig. 10. Measured spectrum of the cogging torque of PMM C.

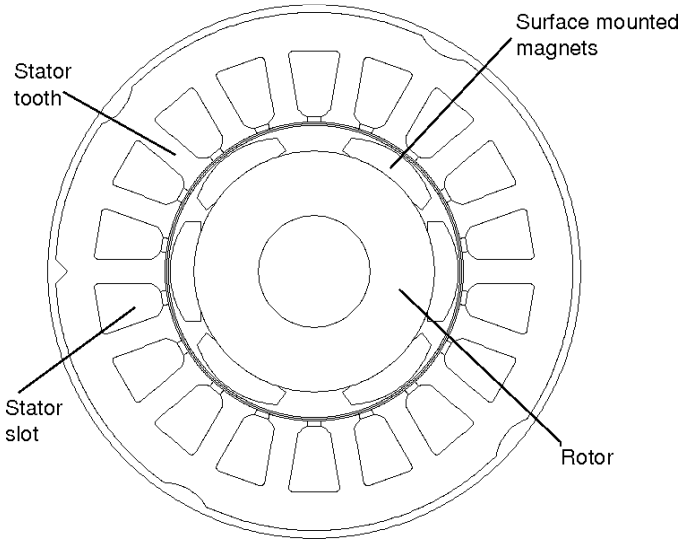

Fig. 11. Lamination of the studied PMM.

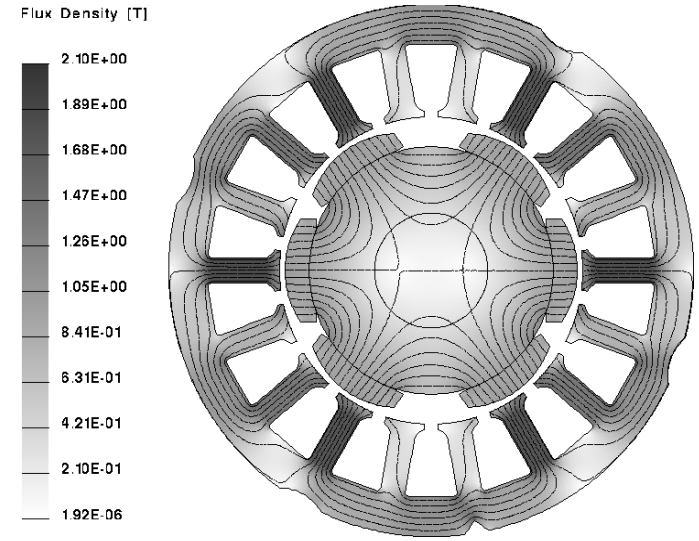

Fig. 12. Flux-density distribution for a single simulation time step.

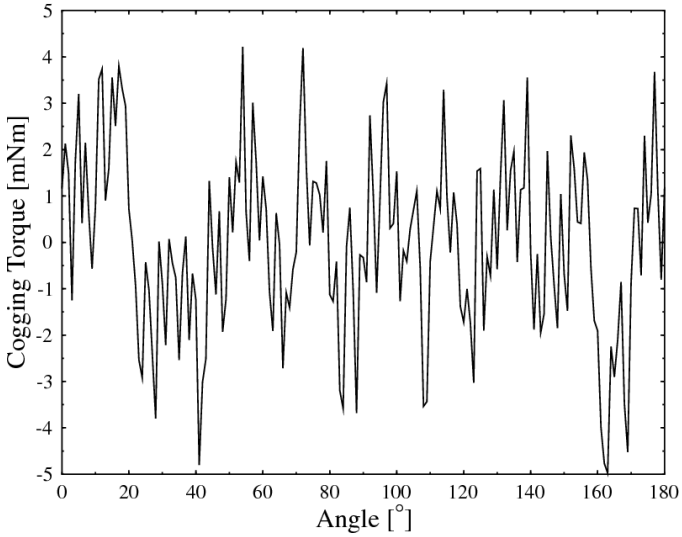

Fig. 13. Time dependent cogging-torque behaviour of the FE-model.

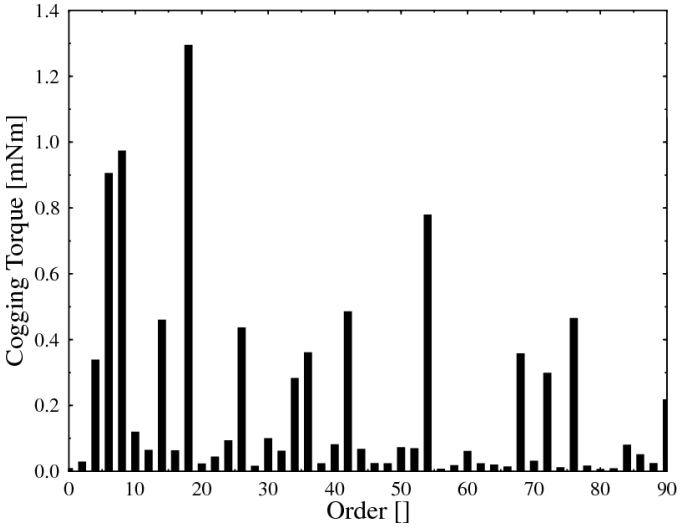

Fig. 15. Spectrum of the cogging-torque harmonics of the FE-model.

is shown in Fig. 11. The permanent magnets are surface mounted, positioned asymmetrically, and shaped. The 2-dimensional FE-model is generated using ANSYS [12]. It consists of about 40.000 triangular elements and 20.000 nodes. As studies have shown, this mesh density suites the task of calculating such small values of cogging torque. For the simulation a static solver is applied taking rotational movement of the rotor into consideration [7]. The stepping angle between two simulation time steps is $\Delta\alpha = 1°$. For each of the 360 simulation time steps the flux density distribution is provided (Fig. 12).

Due to the high magnetization of the magnets (remanence B_R = 1.23 T) the flux density reaches significant saturation values in six of the stator teeth for the depicted rotor position. The mounting kerfs on the outer circumference of the stator are distributed asymmetrically. This results in a slightly asymmetric flux distribution in rotor and stator. Due to this asymmetry cogging torque will appear. Depending on the position of the rotor this cogging torque increases significantly.

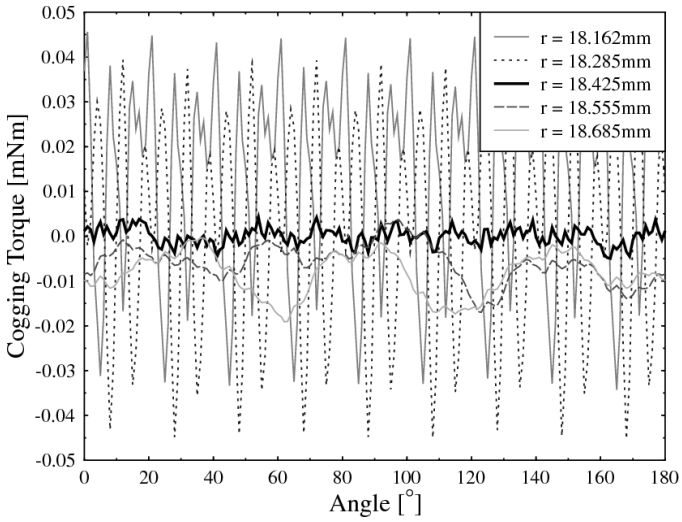

Fig. 14. Time dependent cogging-torque behaviour of the FE-model.

From the flux-density distribution of each simulation time step the cogging torque is calculated. Fig. 13 shows the resulting time depending cogging-torque behaviour. The peak-to-peak value of the cogging torque is ΔT = 9.3 mNm. This states that the studied PMM has been designed very accurately.

When simulating the cogging torque, some considerations have to be taken into account. The torque in the simulation is calculated using the Maxwell's stress tensor:

$$T = \frac{l_m}{\mu_0} \int_\Gamma r \cdot B_r \cdot B_t \cdot \mathrm{d}\Gamma,$$

where B_r and B_t are the radial and tangential component of the flux density, Γ a closed surface around the rotor and l_m the length of the machine. According to [13], the accuracy of torque calculations with Maxwell's stress tensor depends basically on two factors. First, the discretization density must be sufficiently small to be able to resolve the smallest frequency, and yield an accurate solution with a small error. Second, the integration contour position has to be chosen carefully. The air-gap is divided in three layers, which correspond to the stator air-gap, the rotor air-gap and the central air-gap. It is known, that the proximity of the integration contour to the steel can lead to significant errors in the torque calculation. Thus, the central air-gap is chosen to include the integration contour. Nevertheless, significant differences in the torque computation occur if the contour is located close to the border of the air-gap layer. Fig. 14 shows the torque evaluation in different positions in the air-gap. The curve in the center of the results is also the one in the center position in the air-gap. The two positions which are closer to the stator lamination (higher values of r) show a very large content of higher harmonics. Nevertheless, this is not covered by the theory. Thus, the level of confidence of these results is lower. Even comparing the measurement and the simulation for the position in the middle of the air-gap, the content of higher orders is larger in the simulation (see next section). Using the positions closer to the stator, an even higher discrepancy would be obtained. The positions closer to the rotor magnets (smaller values for r in Fig. 14) show clearly the influence of the irregular air-gap

width due to the form of the permanent magnets (see also Fig. 11), and are thus discarded as well. As a result, it can be stated, that a position in the centre of the air-gap should be chosen to evaluate Maxwell's stress tensor. Furthermore, more refined techniques for precise torque estimation could be used in the future [14].

The simulation time step is directly linked to the rotational angle of the rotor. By transforming the cogging torque depending on the angle t he cogging torque is analysed in space domain. Fig. 15 shows the resulting spectrum. As can be observed, the spectrum includes a larger number of higher harmonics than the measured spectrum. This can be due to a number of reasons, discussed in the following section.

V. Discussion

The comparison of the measured and simulated results is depicted in Fig. 16 for the time domain and Fig. 17 for the spectrum (limited to orders up to 40). A reasonably good agreement can be noted. Though, the simulation results are likely to have some room for improvement, especially in the mapping of the higher frequent components. The presence of these higher frequency components can be due to numerical instabilities. Nevertheless, the absence of these components in the measured values can also be due to mechanical damping in the measurement setup. The 18th and 36th order are in very good agreement in the simulation and in the measurement. These are also the orders with the maximum value expected by the theory, as explained in the previous section.

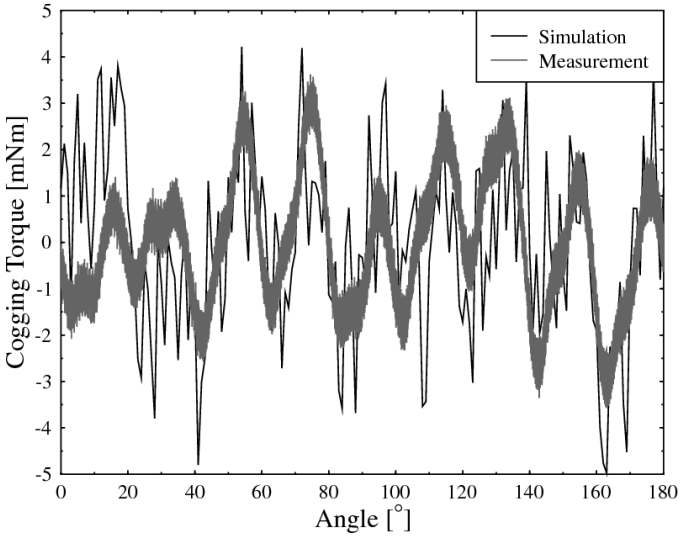

Fig. 16. Comparison of measured an d simulated results in the time domain.

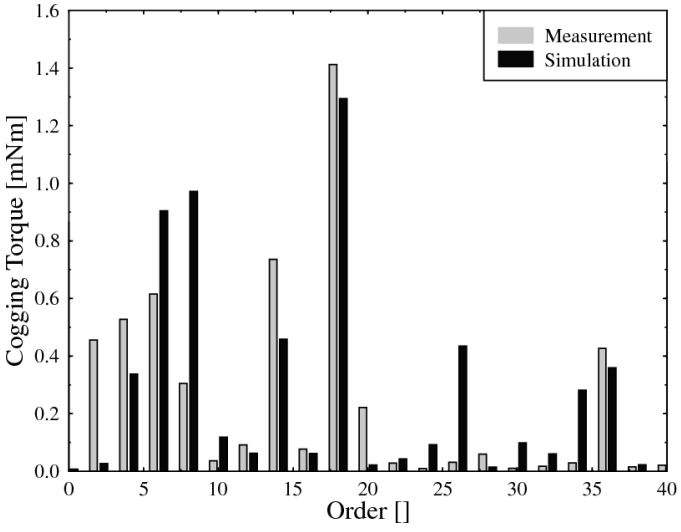

Fig. 17. Comparison of the spectra of measured and simulated cogging torque.

VI. Conclusions

A setup for an accurate cogging torque behaviour assessment through measurements and simulation has been presented. The measured results, in the time and frequency domain, have been compared to simulated results. A good agreement is achieved. The measurement procedure has proven to be an easy and not too expensive, yet accurate way of measuring cogging torques. The simulation results are expected to reach a yet higher accuracy in the near future, by improving the torque calculation further and modelling of more relevant machine details. The applied method allows for an improved design process of PMMs analyzing the cogging torque very easily and accurately.

References

[1] C. Breton, J. Bartolome, J. A. Benito, G. Tassinario, I. Flotats, C. W. Lu, B. J. Chalmers, "Influence of machine symmetry on reduction of cogging torque in permanent-magnet brushless motors," *IEEE Trans. on Magn.*, vol. 36, no. 5, pp. 3819-3823, 2000.

[2] S.-M. Hwang; J.-B. Eom; Y.-H. Jung; D.-W. Lee; B.-S. Kang, "Various design techniques to reduce cogging torque by controlling energy variation in permanent magnet motors," *IEEE Trans. on Magn.*, vol. 37, no. 4, pp. 2806-2809, 2001.

[3] C. S. Koh, "Magnetic pole shape optimization of permanent magnet motor for cogging torque reduction," *IEEE Trans. on Magn.*, vol. 33, no. 5, pp. 1822-1827, 1997.

[4] G. H. Jang, J. W. Yoon, N. Y. Park, S. M. Jang; "Torque and unbalanced magnetic force in a rotational asymmetric brushless DC motors," *IEEE Trans. on Magn.*, vol. 32, no. 5, pp. 5157-5159, 1996.

[5] O. C. Zienkiewicz, R. L. Taylor, *„The finite element method,"* McGraw-Hill Book Company, London, 1989.

[6] A. Kost, *"Numerische Methoden in der Berechnung elektromagnetischer Felder,"* Springer-Verlag, Berlin, Heidelberg, New York, Barcelona, Budapest, Hon Kong, London, Mailand, Paris, Santa Clara, Singapore, Tokyo, 2000.

[7] D. van Riesen, C. Monzel, C. Kaehler, C. Schlensok, G. Henneberger, "iMOOSE-an open-source environment for finite-element calculations," *IEEE Trans. on Magn.*, vol 40, no. 2, pp. 1390 - 1393, March 2004.

[8] F. Aghili, M. Buehler, J. M. Hollerbach, „Experimental Characterization and Quadratic Programming-Based Control of Brushless-Motors," *IEEE Trans. on Cont. Syst. Techn.*, vol. 11, no. 1, pp. 139-146, 2003.

[9] T. Kikuchi, T, Kenjo, "In-Depth Learning of Cogging/Detenting Torque Through Experiments and Simulations," *IEEE Trans. on Edu.*, vol. 41, no. 4, p. 352, 1998.

[10] F. Caricchi, F. G. Capponi, F. Crescimbini, L. Solero, "Experimental Study on Reducing Cogging Torque and No-Load Power Loss in Axial-Flux Permanent-Magnet Machines with Slotted Winding," *IEEE, Trans. on Ind. Appl.*, vol. 40, no. 4, pp. 1066-1075, 2004.

[11] dSPACE, "Solutions for Control," www.dspace.com, *Online*, 2006.

[12] ANSYS Inc., www.ansys.com, *Online*, 2006.

[13] J. Mizia, K. Adamiak et al, "Finite Element Force Calculations: Comparison of Methods for Electric Machines", *IEEE Trans. On Magnetics*, vol. 24, No. 1, Jan. 1988, pp. 447-449.

[14] F. Henrotte, G. Deliège, K. Hameyer.: " The eggshell approach for the computation of electromagnetic forces in 2D and 3D," Compel, Vol.23, N°4, IF 0.180, 2004; pp. 996-1005.